ELSA/7-2012-BGO

Proposal to the PAC

Associated Strangeness Photoproduction with the BGO-OD

The BGO-OD Collaboration

Spokesperson: H. Schmieden, P. Levi Sandri

Contact Person: T.C. Jude, D. Elsner

e-mail: jude@physik.uni-bonn.de, elsner@physik.uni-bonn.de

B. Bantes [1], D. Bayadilov [2], R. Beck [2], M. Becker [2], A. Bella [1], J. Bieling [1], S. Boese [2], A. Braghieri [3], K. Brinkmann [4], D. Burdeynyi [5], F. Curciarello [6,7], V. De Leo [6,7], R. Di Salvo [8], H. Dutz [1], D. Elsner [1], A. Fantini [8,9], T. Frese [1], F. Frommberger [1], V. Ganenko [5], G. Gervino [10,18], F. Ghio [11,12], G. Giardina [6,7], B. Girolami [11,12], D. Glazier [13], S. Goertz [1], A. Gridnev [14], D. Hammann [1], J. Hannappel [1], W. Hillert [1], A. Ignatov [15], O. Jahn [1], R. Jahn [2], R. Joosten [2], T.C. Jude [1], F. Klein [1], K. Koop [2], B. Krusche [16], A. Lapik [15], P. Levi Sandri [17], I. Lopatin [14], G. Mandaglio [6,7], F. Messi [1], R. Messi [8,9], D. Moricciani [8], V. Nedorezov [15], D. Noviskiy [14], P. Pedroni [3], M. Romaniuk [6,7], T. Rostomyan [16], C. Schaerf [8,9], H. Schmieden [1], V. Sumachev [14], V. Tarakanov [14], V. Vegna [1], P. Vlasov [2], D. Walther [2], D. Watts [13], H.-G. Zaunick [2], T. Zimmermann [1]

[1] Physikalisches Institut, Nussallee 12, D-53115 Bonn

[2] Helmholtz-Institut fr Strahlen- und Kernphysik, Nussallee 14-16, D-53115 Bonn

[3] INFN, Sezione di Pavia, via Agostino Bassi 6, 27100 Pavia, Italy

[4] Justus-Liebig-Universitt Gieen, II. Physikalisches Institut, Heinrich-Buff-Ring 16, D 35392 Gieen

[5] National Science Center Kharkov Institute of Physics and Technology, Akademicheskaya St. 1, Kharkov, 61108, Ukraine

[6] Dipartimento di Fisica e di Scienze della Terra, Università di Messina, v.le F. Stagno d'Alcontres 31, 98166 Messina, Italy

[7] INFN, Sezione di Catania, via Santa Sofia 64, 95123 Catania, Italy

[8] INFN, Sezione di Roma "Tor Vergata", Via della Ricerca Scientifica 1, 00133 Roma, Italy

[9] Dipartimento di Fisica, Università di Roma "Tor Vergata", via della Ricerca Scientifica 1, 00133 Roma, Italy

[10] Dipartimento di Fisica, Università di Torino, via P. Giuria 1, 10125 Torino, Italy

[11] INFN, Sezione di Roma, c/o Dipartimento di Fisica - Università di Roma "La Sapienza", P.le Aldo Moro 2, 00185 Roma, Italy

[12] Istituto Superiore di Sanità, viale Regina Elena 299, 00161 Roma, Italy

[13] The University of Edinburgh, James Clerk Maxwell Building, Mayfield Road, Edinburgh EH9 3JZ UK

[14] Petersburg Nuclear Physics Institute, Gatchina, Leningrad District, 188300 Russia

[15] Russian Academy of Sciences Institute for Nuclear Research, prospekt 60-letiya Oktyabrya 7a, Moscow 117312 Russia

[16] Institut fr Physik, Klingelbergstrasse 82, CH-4056 Basel

[17] INFN - LNF, Via E. Fermi 40, 00044 Frascati (Roma), Italy

[18] INFN, Sezione di Torino, via P. Giuria 1, 10125 Torino, Italy

Bonn, November 5, 2012

Abstract

A series of experiments for the investigation of associated strangeness photoproduction are planned for the BGO-OD experiment. This proposal includes two dedicated beam time requests:

1. To measure $\gamma p \to K^+\Lambda$ differential cross section from threshold to 2.88 GeV photon beam energy over a large angular acceptance range. The measurement will cover the structure at $W = 1.9$ GeV, where discrepancies in the world data set have lead to ambiguities in partial wave analysis, and also cover very forward regions with high precision where there is limited data.

2. To measure the beam asymmetry, Σ for $\gamma p \to K^0\Sigma^+$ over the photon beam energy range 1680-1845 MeV. The measurement will be the first Σ data for this channel over this energy range, covering the K^* threshold region in which a "cusp" structure is observed in the $K^0\Sigma^+$ differential cross section. It is speculated that this cusp structure is due to sub-threshold K^* production rescattering into this channel, which is then absent above K^* threshold. Such mechanisms could also be regarded as dynamically generated hadronic states. Beam asymmetry measurements over the K^* production threshold will shed light on the reaction mechanism.

Analysis of these channels will form the foundation for the next set of experiments, the motivations of which are outlined in this proposal: Polarisation observables and differential cross section data for $\gamma n \to K^0\Lambda$, and the investigation into missing or poorly understood hyperon resonances.

Equipment

Both experiments will be performed at the ELSA accelerator using the BGO-OD setup and a liquid hydrogen target. For the first request, unpolarised electrons with an energy of 3.2 GeV are required. Using a copper radiator, this will provide a photon flux of 5×10^6 s^{-1} from 911 MeV (threshold) to 2.88 GeV. The second request requires an electron beam at an energy of 3.2 GeV and a crystal radiator to produce linear polarised photons over the range 1680-1845 MeV. This equates to a photon flux over this range of 2.53×10^5 s^{-1}, with a conservative estimation of 30% polarisation.

Accelerator & target specification

e^- beam:	3.2 GeV e^- unpolarized
beam line:	BGO-OD experimental area
beam intensity:	Request 1: $5{\cdot}10^6$ photons/s in the energy range 0.91 - 2.88 GeV
	Request 2: $2.53{\cdot}10^5$ photons/s in the energy range 1.68 - 1.85 GeV
polarization:	Request 1: No polarisation
	Request 2: Linear polarised beam, maximum polarisation at 1.80 GeV
target:	LH_2
trigger:	BGO or forward spectrometer

beamtime request

Request 1: LH_2: **1000 h**. Request 2: LH_2: **2000 h**

Contents

List of Figures

List of Tables

1 Introduction

With the advent of higher duty factor accelerators delivering photon beams over the comparitively large associated strangeness production threshold ($\sim$ 1 GeV) over the last 10-15 years, differential cross section and polarisation observable data for channels with open strangeness has markedly increased. Despite these advances, there are still many open questions in associated strangeness photoproduction. For charged kaon photoproduction, partial wave analyses of the world data are unable to agree on the contributions of s-channel resonances in the photoproduction mechanism. Neutral kaon photoproduction is an important constraint to understand the reaction mechanism. The absence of t-channel pseudoscaler kaon exchange renders K^0 photoproduction an important probe into into the role of K^* t-channel exchange. It also allows a "cleaner" spectrum of s-channel resonances in the excitation spectrum, where t-channel processes can dominate charged kaon photoproduction.

The BGO-OD experiment, with the BGO calorimeter and forward spectrometer at forward angles provides unique opportunities for the investigation for associated strangeness photoproduction. Data at very forward angles can be taken with high momentum precision using the forward spectrometer,

which, for example, is essential to determine t-channel contributions. The complementarity of a large acceptance segmented calorimeter (BGO) with additional charged particle identification (MWPC and inner plastic scintillator) allows the identification of final states with mixed charges and the ability to identify particles via different decay mechanisms, improving statistics for the analysis of channels with low cross sections. The identification of mixed final states is also important for the investigation into hyperon (Y^*) states, where for example, all three decay modes can be detected for $\Lambda(1405) \rightarrow \Sigma\pi$.

The programme of measurements with the BGO-OD is extensive and so the beam time requested in this proposal concentrates on the first chapter of measurements and is as follows. Section 2 describes the physics motivations for the first set of experiments with charged and neutral kaon photoproduction. Section 3 describes the BGO-OD experiment and section 4 presents simulated data analysis, estimated count rates and beam time requests. Section 6 is an outlook at the next set of experiments for the associated strangeness programme.

2 Physics motivation

2.1 $\gamma p \rightarrow K^+\Lambda$

$\gamma p \rightarrow K^+\Lambda$ has the lowest energy threshold for photoproduction reactions with final state particles containing strange valence quarks. This is a crucial channel for investigation as many models predict poorly established or "missing" resonances couple strongly to strange decay channels [1]. The Λ weak decay also allows access to its polarisation from the distribution of its decay particles ensuring that $\gamma p \rightarrow K^+\Lambda$ will be the first photoproduction reaction with a complete measurement of observables and will be a benchmark channel for partial wave analysis (PWA) studies.

Detailed measurements of $\gamma p \rightarrow K^+\Lambda$ from threshold have been obtained with the SAPHIR [2, 3] and CLAS detectors [4, 8]. Unfortunately the cross section data have discrepancies which lead to significant differences in the PWA solutions using either data set (see [6] for a brief review). The most notable difference is around the structure at $\sqrt{s}$ = 1.9 GeV. The LEPS collaboration [7] measured the $K^+\Lambda$ differential cross section for centre of mass energies 1.945-2.28 GeV (photon beam energy of 1.5-2.4 GeV) and forward angular range (centre of mass K^+ polar angle of $0 - 60^0$). The data was consistent with the CLAS data in the energy overlap region (see fig. 1) and partially reproduces the peak structure at $\sqrt{s}$ = 1.9 GeV, however this is at the lower limit of the energy range. The data extends beyond the angular acceptance of the CLAS data (approximately 25^0 in the centre of mass).

Recent photoproduction data has indicated narrow structure in a number of sources, for example in η photoproduction off the neutron [9, 10], although the interpretation remains controversial. Narrow resonance states [11] and coupled channel effects [12] have both been suggested as mechanisms for creating this structure. Accurate $\gamma p \rightarrow K^+\Lambda$ data has been proposed as a powerful tool to help settle this fundamental issue [13]. A recent second analysis of CLAS data has extended the kinematic range to lower energies at more backward angles (fig. 2) [14, 15]. Large peaked structure was observed at $\sim$ 1670 MeV, which has been interpreted as N(1710)$1/2^+$ and N(1720)$3/2^+$ [14] however has not been observed in any previous $K^+\Lambda$ analyses.

2.2 $\gamma p \rightarrow K^0\Sigma^+$

Fig. 3 shows $\gamma p \rightarrow K^0\Sigma^+$ differential cross section measured by Ewald *et al* [16] with the Crystal Barrel detector at ELSA. Directly above the $K^0\Sigma^+$ threshold a differential cross section of $\simeq 0.02\,\mu$barn/sr is obtained with flat angular dependence, typical for s-wave production. The cross section rises with increasing photon energy and also develops an increasing forward peaking, suggesting increasing t-channel contributions.

A pronounced structure is found in the vicinity of the K^* thresholds. In forward directions the differential cross section drops by a factor of 4, and up to the highest measured energies an almost flat angular distribution is then obtained. The effect is strong enough to become clearly visible in the total cross section, cf. Fig. 4(left).

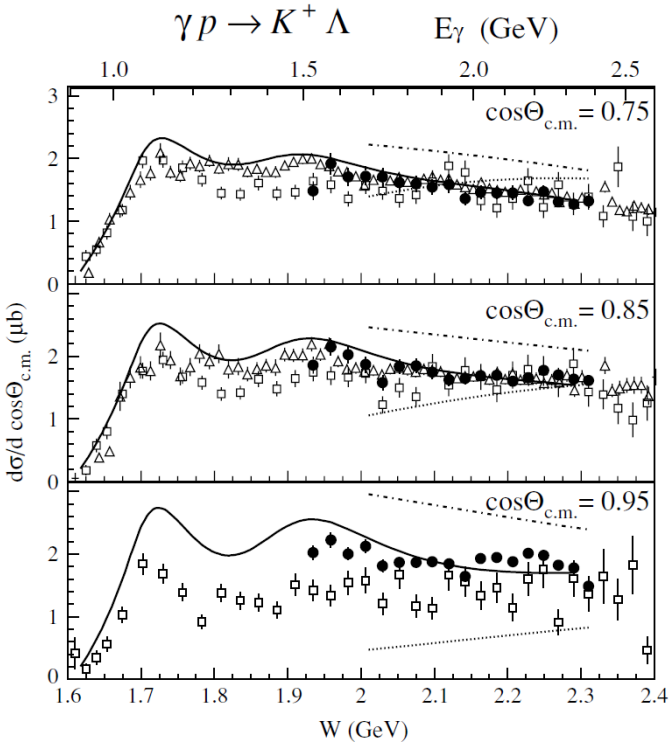

Figure 1 $\gamma p \to K^+\Lambda$ differential cross sections. Closed circles LEPS [7], open squares SAPHIR [2], triangles CLAS [4, 5].

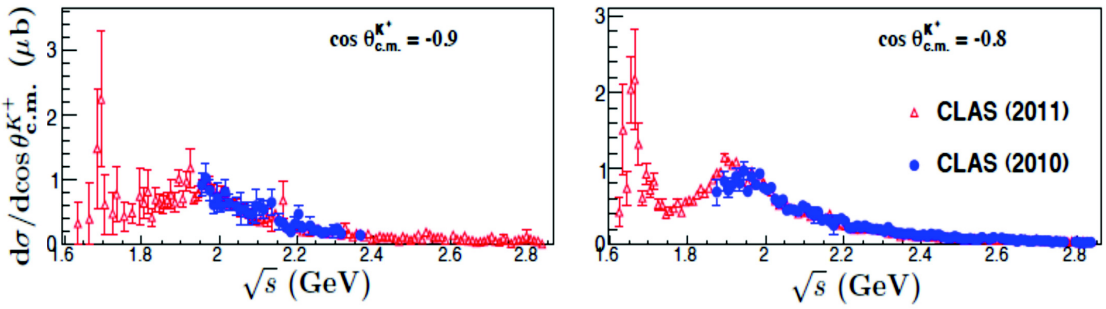

Figure 2 Analysis of $\gamma p \to K^+\Lambda$ differential cross section data from CLAS, with $K^+p\pi^-$ topology (blue) and K^+p or $K^+\pi^-$ topology (red). Taken from [14].

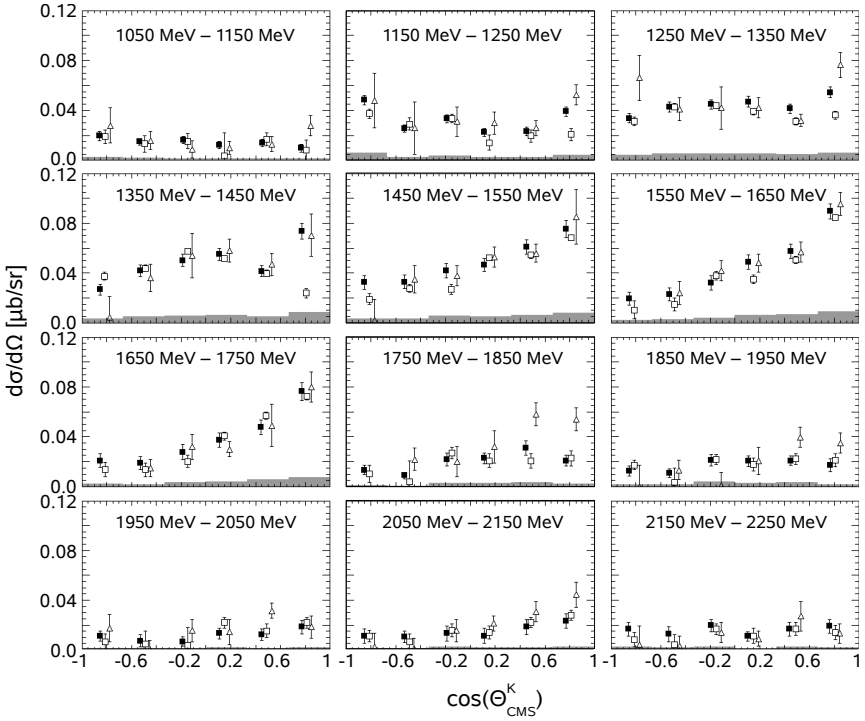

Figure 3 Measured differential cross sections for $K^0\Sigma^+$ photoproduction as a function of the kaon centre-of-mass angle in ± 50 MeV wide bins of photon energy from 1100 to 2200 MeV. The present results (full squares) are compared to previous measurements of Crystal Barrel (open squares) [21] and SAPHIR (triangles) [22]. The error bars are purely statistical. An estimate of the systematic uncertainty is given by the bars on the abscissa.

The structure seems related to a change in the reaction mechanism in the vicinity of the K^* threshold. The role of K^*-exchange (fig. 5a) was investigated using K-MAID [17] where it is possible to manually change the K^* exchange strength. With standard parameters both, K-MAID and SAID [18], deliver an unsatisfactory description of the data, cf. the dashed and dashed-dotted curves in Figure 4, respectively. Below the K^* threshold this can be drastically improved by adjusting the couplings of the $S_{31}(1900)$ state to $G_1 = 0.3$ and $G_2 = 0.3$ and reduction of the Born-couplings from 1 to 0.7.

Two versions (for details see [16]) of K-MAID are depicted in fig. 4. The inclusion of K^*-exchange improves the description of the data below K^* threshold. Contrary, omission of K^*-exchange renders K-MAID closer to the data above the threshold. At the K^* threshold the K-MAID variants with and without K^*-exchange exhibit a difference of the order of the observed drop.

This leads to the following speculation. In diagram (b) and (c) of fig. 5 no real K^{*0} or K^{*+} is produced below K^* threshold. However, in the vicinity of the K^* threshold a $K^{*0,+}$ would be produced almost on mass shell. It then strongly couples to a K^0 and a charged or neutral pion. In this way a rescattering of the type 5(b) and (c) may contribute to the K^0 channel.

Such a contribution will vanish from the K^0 channel once the K^* is produced as a free particle above its reaction threshold, then contributing to the $K^{*0}\Sigma^+$ channel. The strength, which at the dip of the cross section is taken from the K^0 channel, should then show up in $K^{*0}\Sigma^+$. In order to test this idea, the measured total cross section of the reaction $\gamma p \to K^{*0}\Sigma^+$ [19] was added to the observed $K^0\Sigma^+$ cross section above the K^* threshold. The result is shown in fig. 4(left) (grey circles). The sum of the two cross sections indeed exhibits a smooth transition from below to above the K^* thresholds and the dip structure vanishes.

The loops in fig. 5(b) and (c) could be regarded as dynamically generated $(K^*\Sigma)^+$ or $(K^*\Lambda)^+$ states in the vicinity of the K^* threshold. Such states are expected in chiral unitary approaches through the interaction of the nonet of vector mesons with the octet of baryons. In Ref. [20] a non-strange isospin $1/2$ doublet is indeed predicted at a mass of 1972 MeV, i.e. very close to the K^* threshold. Experimentally, the reaction mechanism can be further constrained through polarisation observables.

Unfortunately, the beam asymmetry was only measured below the K^* threshold (up to a beam energy of 1650 MeV) [16]. Nevertheless, an interesting effect is observed regarding the hypothesised reaction mechanism.

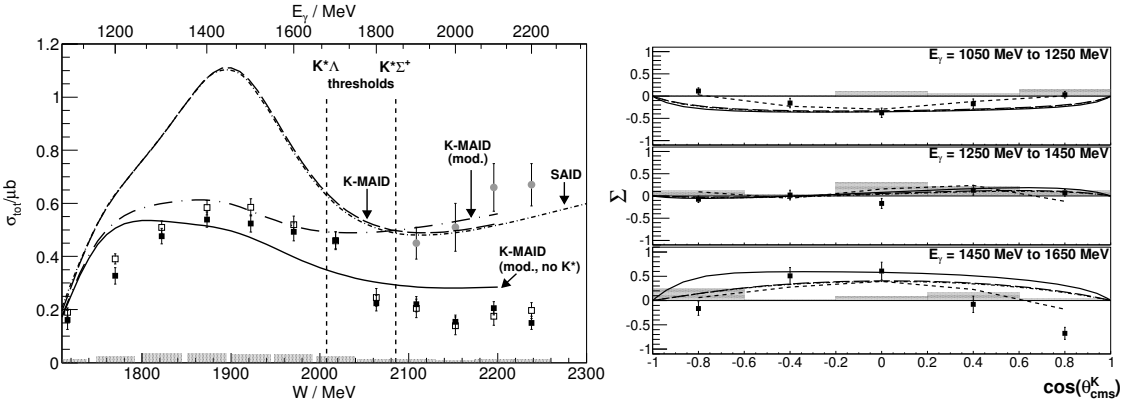

Figure 4 **left:** Total cross section for $K^0\Sigma^+$ photoproduction as a function of the centre-of-mass energy from the present experiment (full squares) in comparison to the previous Crystal Barrel (open squares) [21] data. The vertical lines indicate the $K^*\Lambda$ and $K^*\Sigma^+$ thresholds at $W = 2007.4$ and 2085.5 MeV, respectively. The SAID parameterisation [18] is represented by the short dashed-dotted curve. A K-MAID calculation [17] with standard parameters yields the dashed curve. The long dashed-dotted curve is obtained from K-MAID with the modifications described in the text, and standard K^*-exchange included. The full curve has the same modifications, but K^*-exchange excluded. Above the K^* threshold the grey circles represent the sum of the cross sections of $K^0\Sigma^+$ of the present experiment and $K^{*0}\Sigma^+$, also measured by Crystal-Barrel/TAPS [19]. The vertical bars on the abscissa indicate the systematic error of the present experiment, the errors plotted with the data symbols are purely statistical. **right:** Angular distribution of the photon beam asymmetry Σ_γ in the three bins of photon energy indicated in the diagrams. The error bars attached to the data points are purely statistical. The systematic errors are indicated by the grey bars on the abscissa. Curves shown represent: SAID [18] (dash-dotted) and K-MAID (long-dashed) [17] with standard parameters, K-MAID with parameters modified as explained in the text (full), and Bonn-Gatchina PWA (short-dashed).

Accounting for a linearly polarised photon beam, the cross section of photoproduction of pseudoscalar mesons off a nucleon can be written in the form

$$\frac{d\sigma}{d\Omega} = \left(\frac{d\sigma}{d\Omega}\right)_0 (1 - P_{\mathrm{lin}}\Sigma_\gamma \cos 2\phi) \tag{1}$$

with polarisation independent cross section, $(d\sigma/d\Omega)_0$, degree of linear polarisation, P_{lin}, and photon beam asymmetry, Σ_γ. The product $P_{\mathrm{lin}}\Sigma_\gamma$ determines the magnitude of modulation of the cross section with the azimuthal angle ϕ beween the plane of linear polarisation and the ejected meson. Vice versa, the product is obtained from the measured modulation by a fit of a $\cos 2\phi$ function to the K^0 yield, from which Σ_γ can then be determined using the known beam polarisation. The results for the beam asymmetries are presented in fig. 4(right).

At threshold the photon beam asymmetry is negative[a] and compatible with zero throughout the intermediate energy bin. At higher energies the beam asymmetry changes sign and turns clearly positive, except at forward directions where it becomes strongly negative. The highest energy bin is still below the K^* thresholds which is at $E_\gamma = 1678.2$ MeV for the $K^{*+}\Lambda$ final state, and at $E_\gamma = 1848.1$ MeV for $K^{*0}\Sigma^+$.

The parameterisations of the photon beam asymmetry show reasonable agreement with the Crystal Barrel data, except in forward directions in the highest energy bin. Interferences of partial waves ren-

[a] note that it is bound to zero at $|\cos\theta| = 1$

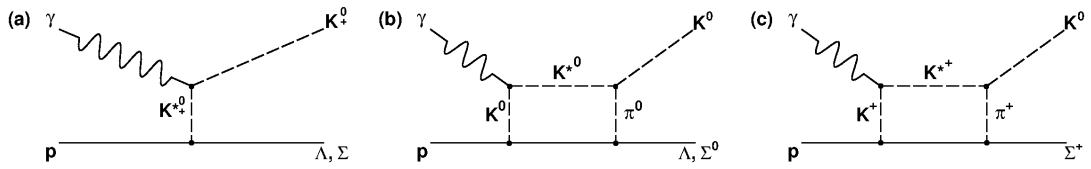

Figure 5 Mechanisms for kaon photoproduction, descriptions in the text.

der the beam asymmetry very sensitive to resonances in s-channel production. In t-channel processes, however, the photon beam asymmetry reflects the character of the t exchange. The dominant parts of the electromagnetic coupling with the t-exchange are $T(K^*) \propto (\vec{\epsilon} \times \vec{q}) \cdot \vec{p}_f$ and $T(K) \propto \vec{\epsilon} \cdot (\vec{q} + \vec{p}_f)$ for K^* and K exchange, respectively, with the photon polarisation vector, $\vec{\epsilon}$, and the momenta of the exchanged (intermediate) and final-state kaons, $\vec{q}$ and $\vec{p}_f$. The scattered kaon and hyperon in the final state are produced most likely perpendicular to the plane of photon polarization when a K^* is exchanged, and parallel to it in the case of an intermediate K. With the cross sections perpendicular ($\sigma_\perp$) and parallel ($\sigma_\parallel$) to the photon polarisation plane, the photon beam asymmetry is defined as $\Sigma = \frac{\sigma_\perp - \sigma_\parallel}{\sigma_\perp + \sigma_\parallel}$. In the case of a K^* exchange the asymmetry is therefore expected to be positive and, oppositely, negative for a pseudoscalar K.

In the highest energy bin, where t-exchange is dominant, the beam asymmetry is generally positive compatible with K^{*0}-exchange. In forward directions of the 1450–1650 MeV bin, however, it turns significantly negative. This indicates the predominant exchange of a pseudoscalar K, and due to stronger charge coupling very probably a K^+. Hence, the beam asymmetry seems to support a t-channel mechanism with subsequent rescattering as shown in fig. 5(b,c). It appears compatible with the above speculation on the origin of the strong downturn of the forward cross sections. To further study this it will be necessary to extend the beam asymmetry measurements beyond the K^* threshold.

Extending the measurements of the beam asymmetry to energies across the K^* threshold will probe the role of t-exchange.

3 The BGO-OD experiment

The BGG-OD detector setup is a combination of a central detector system and a forward spectrometer for charged particles, completed by a photon tagging system.

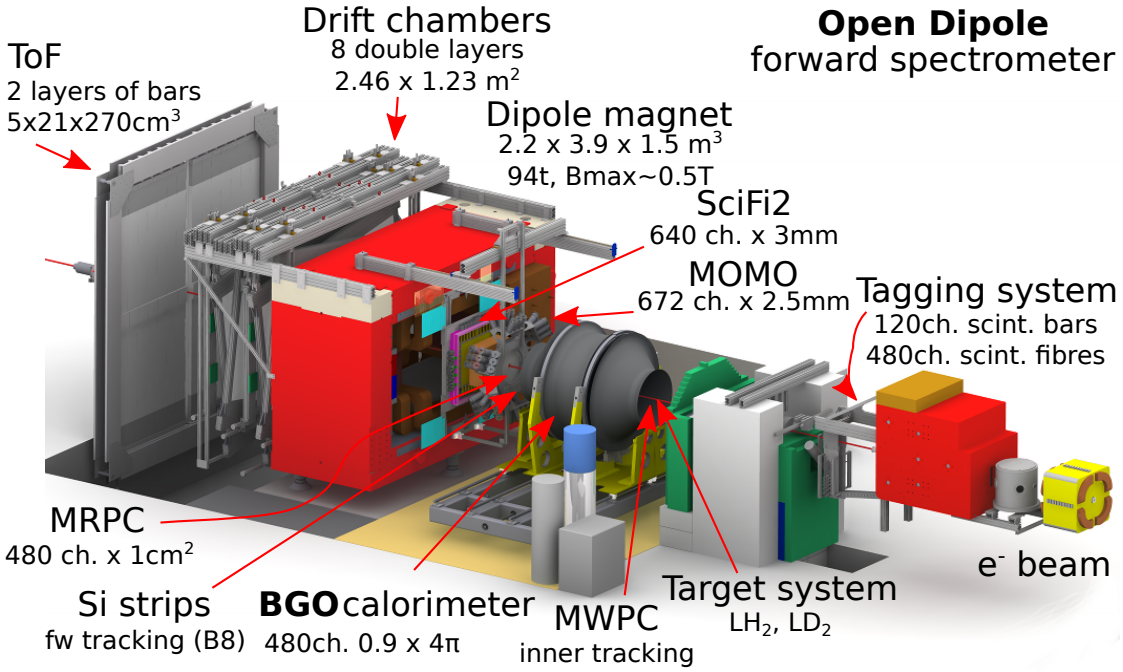

Figure 6 The BGO-OD experimental setup

The central detector of the experimental setup is the high resolution and large solid angle ($0.9 \cdot 4\pi$) BGO[b] electromagnetic calorimeter of the former GRAAL experiment [23, 24, 25, 26]. The calorimeter is

[b] $Bi_4Ge_3O_{12}$

combined with two multi-wire proportional chambers (MWPC) for inner tracking and a plastic scintillator barrel for particle identification through the measurement of dE/dx. The calorimeter consists of 480 BGO crystals with a length of 24cm ($>$ 21 radiation lengths).

The region between the acceptance of the central detector and the forward spectrometer will be covered by an azimuthally symmetric Multi-gap Resistive Plate Chamber (MRPC), which is a contribution from external BGO-OD collaborators (INFN Rome and University of Rome). The MRPC will be located between the BGO calorimeter and the MOMO detector.

The forward spectrometer is based on a large open dipole magnet, a permanent loan by DESY. Tracks are reconstructed in front of the magnet by two fiber hodoscopes, MoMo and SciFi2.

Behind the magnet tracking is done using a set of 8 double layer drift chambers in four different orientations, vertical wires to measure the x-coordinate, horizontal for the the y-coordinate, and tilted by $\pm 9^\circ$ from vertical, for a u- and v-coordinate.

The forward spectrometer is completed by a set of time-of-flight walls that are used to discriminate the various particles.

The photon tagging system, uses a series of 120 adjacent, partially overlapping plastic scintillators with fast photomultiplier readout. It is designed to cover an electron energy range between 10% and 90% of the ELSA energy. In 2003 an additional scintillating fibre hodoscope will be added to allow the precise determination of the degree of polarisation for linearly polarised photons by measuring the shape of the coherent edge.

Part	Acceptance	angular resolution	time resolution	p/E resolution
BGO Ball	$25^\circ < \Theta < 155^\circ$	$\Delta\Theta < 6^\circ$,$\Delta\Phi < 7^\circ$	$< 3\,\mathrm{ns}$	$\approx 3\,\%$ for 1 GeV photons
MWPC	$18^\circ < \Theta < 163^\circ$	$\Delta\Theta \approx 1^\circ$,$\Delta\Phi = 2^\circ$	n.a.	n.a.
MRPC	$8^\circ < \Theta < 25^\circ$	$< 1^\circ$	50 ps	n.a.
forward spec.	$\Theta_{vert} < 8^\circ$	$\Delta\Theta_{\Theta<4^\circ} < 0.2^\circ$	n.a.	$< 3\,\%$ for $p < 1.5\,\mathrm{GeV}$
	$\Theta_{hor} < 12^\circ$	$\Delta\Theta_{\Theta<10^\circ} < 0.3^\circ$	n.a.	$< 6\,\%$ for $p < 3\,\mathrm{GeV}$
ToF	$\Theta_{vert} < 8^\circ$,$\Theta_{hor} < 12^\circ$		500 ps	n.a.
Tagger	n.a.	n.a.	275 ps	10 MeV to 40 MeV

Table 1 Parameters of the BGO-OD setup

4 Experimental approach and count rate estimates

This section comprises two parts. Section 4.1 describes the experimental approach and count rate estimates for $\gamma p \rightarrow K^+\Lambda$ analysis. This includes a new method of K^+ identification via the weak decay in the BGO crystals, and a method of separating $K^+\Lambda$ and $K^+\Sigma^0$ channels via the identification of the photon from the Σ^0 radiative decay. The simulated analysis is then used to estimate the beam time required to measure the differential cross sections for a given precision.

Section 4.2 describes the methods that will be used to identify K^0 and a calculation of the beam time required to perform the asymmetry measurements.

An accurate Geant4 [27] simulation of the BGO-OD experiment has been used to determine detection efficiencies. The analysis procedure of the simulated data includes all sub-detectors of the BGO-OD experiment and is able to reconstruct particles in the final state. The generated events follow SAID solutions [18] folded with a $1/E_\gamma$ bremsstrahlung distribution

The same analysis procedures have already been used with experimental commissioning data and it is anticipated that this will also be the foundation for the analysis of the proposed experiments.

As there is no current analyses with the BGO-OD experiment, the simulated data has no direct comparison, and so should only be regarded as estimates. It is encouraging however that extracted detection efficiencies are close to those extracted with similar experimental conditions (K^+ identification with the Crystal Ball and K^0 neutral decay identification with the Crystal Barrel).

4.1 $\gamma p \to K^+\Lambda$

4.1.1 K^+ identification in the BGO

A new method of K^+ identification has been developed by identifying the time delayed weak decay of K^+ within the crystals of the BGO. The energy deposited during the decay of a stopped K^+ (150 MeV for $K^+ \to \mu^+\nu_\mu$ or up to 350 MeV for $K^+ \to \pi^+\pi^0$) spoils the particle signature expected with the inner plastic scintillator. As the K^+ has a lifetime of 12 ns however, an incident cluster of adjacent crystals with energy deposition can be split into two: A first sub-cluster from the kinetic energy of the K^+, and a second sub cluster from the energy of the decay products. The sub-clusters were created by grouping crystals within a cluster into a sub-cluster if the time of energy deposition was within 8 ns. A final selection cut with the inner plastic scintillator rejected background of low energy electrons.

The method was tested extensively with simulated data (fig. 7). Fitting an exponential function to the time difference of the two sub-clusters yields the expected K^+ lifetime of $\sim$ 12 ns (fig. 7 left) and the energy of the 2nd sub-cluster is consistent with the 150 MeV energy release for the decay $K^+ \to \mu^+\nu_\mu$ (fig. 7 right).

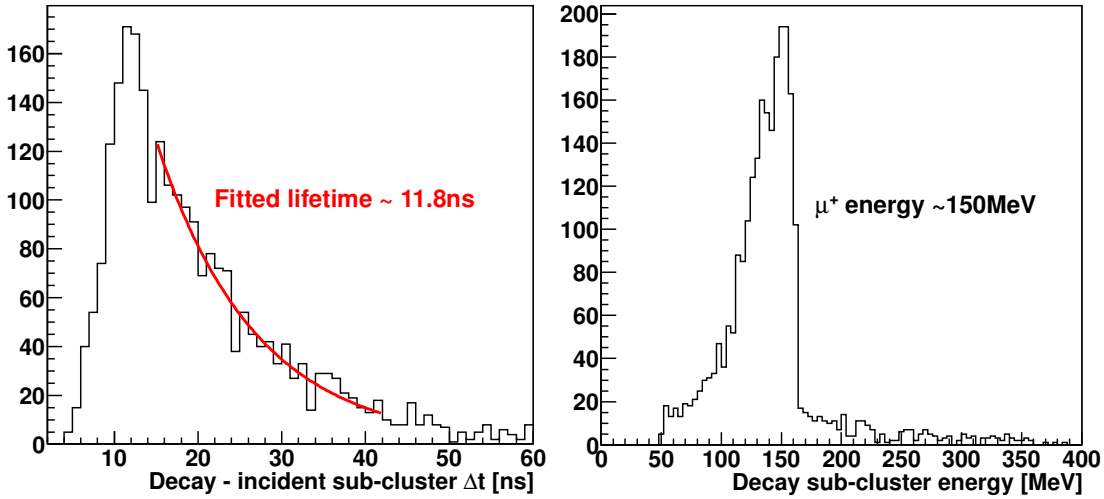

Figure 7 Identification of the K^+ weak decay within the BGO crystals. Left, time between 1st and 2nd sub-cluster, right: energy of the 2nd subcluster. Description in the text.

Data from a commissioning beam time in March 2012 demonstrates the first evidence of K^+ identification with experimental data (fig.8). The data set had no charged particle identification, resulting in the tail rising towards the low energy part of the spectrum.

$\gamma p \to K^+\Lambda$ will be identified by the missing mass of the recoiling hyperon from the K^+ in the final state. Fig. 9 shows this plot for K^+ identified in the forward spectrometer and the BGO for both $K^+\Lambda$ and $K^+\Sigma^0$. Below a beam energy of 2 GeV, the two channels are completely separable for K^+ identified in the forward spectrometer. For the BGO and the forward spectrometer at energies above 2 GeV however, the missing mass spectra of the channels overlap. The events can still be separated however with negligible yield loss via the detection of the photon from the decay $\Sigma^0 \to \Lambda\gamma$. Fig 10 is the photon energy in the hyperon rest frame versus the missing mass from the combined K^+ and γ four momenta. A peak is evident at the $\Sigma^0 - \Lambda$ mass difference.

The $\gamma p \to K^+\Lambda$ detection efficiency is shown in fig. 11. At forward angles, the forward spectrometer provides a detection efficiency of 60-70% and at more backward angles the BGO provides an efficiency of 10-15%.

The MWPC within the BGO will be commissioned before the requested beam time. This will enable Λ to be identified via the detached decay vertex, and provide a second method to identify this channel. This will provide a check of analysis techniques and increase the angular acceptance. Fig. 12 shows the range of W and K^+ centre of mass polar angle accesible if the Λ is identified with the MWPC.

The following beam time request only uses detection efficiencies based upon the direct detection of K^+ either in the BGO or the forward spectrometer only.

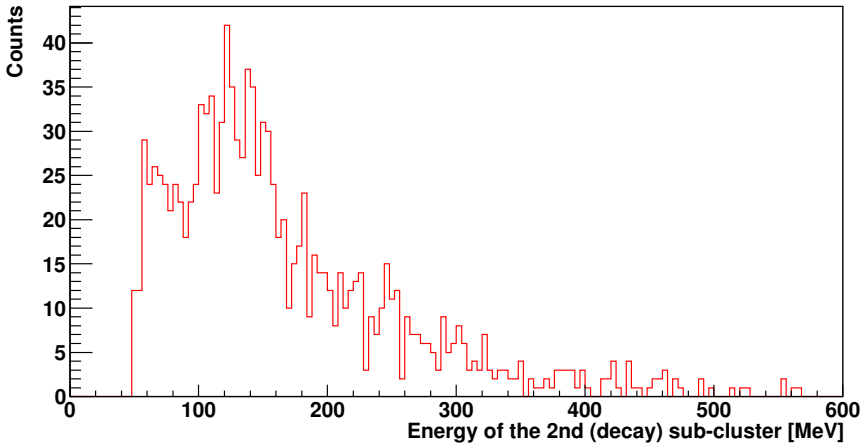

Figure 8 Identification of the K^+ weak decay within the BGO crystals. With experimental data. No charged particle identification was used

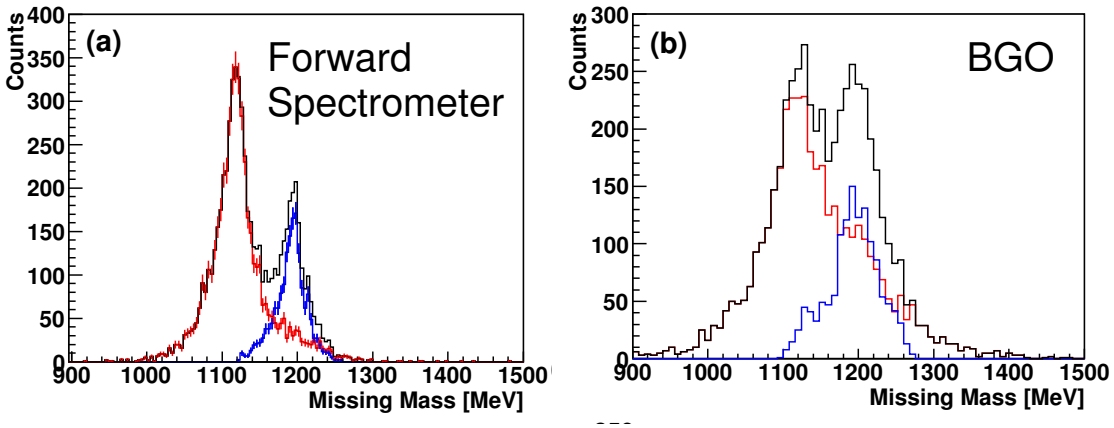

Figure 9 Missing mass for the detected K^+ in (a) The forward spectrometer and (b) the BGO. Black line is simulated data for both $K^+\Lambda$ and $K^+\Sigma^0$. The channels were separated (red and blue lines) by the identification of the Σ^0 radiative decay (described in the text).

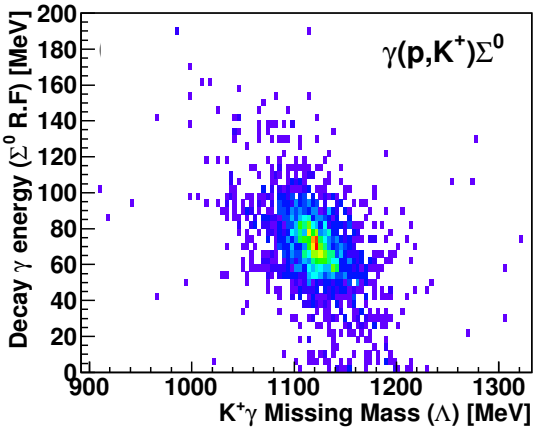

Figure 10 Detected photons in the Σ^0 rest frame (simulated data). For the decay $\Sigma^0 \to \gamma\Lambda$, γ energy is equal to the $\Sigma^0 - \Lambda$ mass difference (77 MeV) (y-axis). $K^+\gamma$ missing mass yields the Λ mass of 1116 MeV (x-axis).

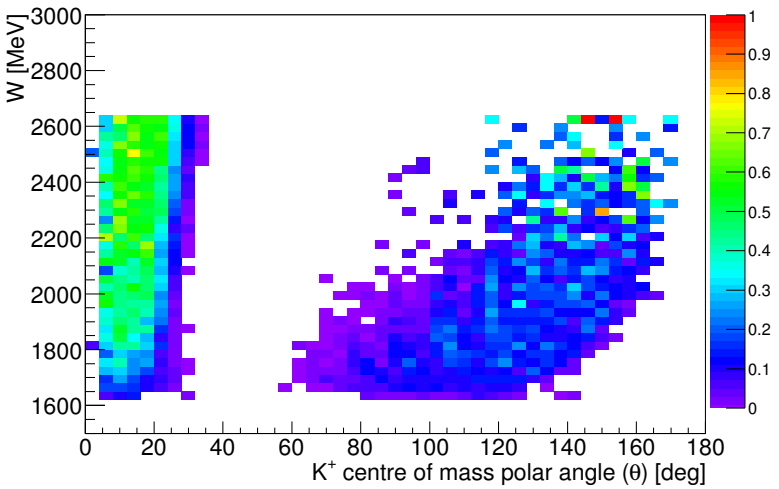

Figure 11 Detection efficiency for $\gamma p \rightarrow K^{+}\Lambda$.

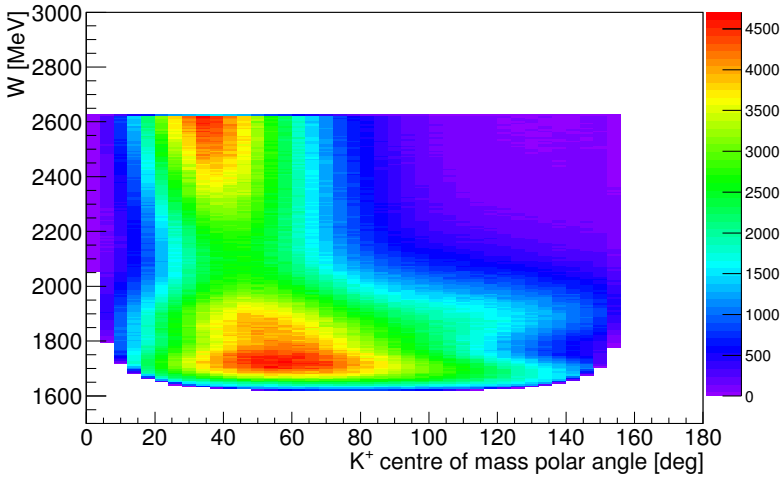

Figure 12 K^{+} acceptance region for when Λ are identified in the MWPC via the detached decay vertex. Distributions follow a SAID solution folded with the $1/E$ bremsstrahlung spectrum.

4.1.2 Beam time request

- N_θ = number of bins in centre of mass polar angle = 14;
- N_W = number of bins in centre of mass energy, W = 40;
- ΔA = the statistical precision required = 0.05 of the measured cross section;
- $d\sigma/d\Omega$ = approximate differential cross section $\approx$ 0.1 μb;
- N_γ = photon flux [s^{-1}] $\approx 5 \times 10^6$ from 0.911-2.88 GeV;
- ρ_T = Target surface density = 0.2558 b^{-1};
- ϵ_{eff} = detection efficiency multiplied by solid angle of acceptance = 0.1$\times$11.3 for the BGO + 0.25$\times$0.06 for the forward spectrometer;
- ϵ_{DAQ} = data taking running efficiency = 0.5 (macroscopic duty factor of the ELSA beam (0.714), DAQ lifetime (0.75) and a small safety margin (0.93)).

The estimated beam time required, t is given as:

$$t = \frac{N_\theta N_W}{\Delta A^2 (d\sigma/d\Omega) N_\gamma \rho_T \epsilon_{eff} \epsilon_{DAQ}}$$

A beam time of 1000 hours ($\sim$42 days) with an unpolarised beam to a photon energy of 2.88 GeV (electron beam energy of 3.2 GeV) is therefore requested.

4.2 $\gamma p \to K^0\Sigma^+$

4.2.1 K^0 identification with the BGO-OD

Fig. 13(a) and (c) show the reconstruction of the K^0 invariant mass by the identification of the decay $K^0 \to \pi^0\pi^0$. Accounting for the decay branching ratio, this has a detection efficiency of approximately 4%. The decay $K^0 \to \pi^-\pi^+$ can also be used to reconstruct the K^0 invariant mass, however the small acceptance of determining the π^- momentum in the forward spectrometer renders the detection efficiency very small.

Fig. 13(b) and (d) show the reconstruction of the Σ^+ invariant mass via the decay $\Sigma^+ \to p\pi^0$. This has an efficiency of approximately 7%. To reduce background from other channels, this can be used in conjunction with identification of the decay $K^0 \to \pi^-\pi^+$, and fixing the π^- momentum from the other known four momenta. The charged decay has a detection efficiency of approximately 70%, reducing the combine detection to approximately 5%.

Combining both methods of detection yields a total detection efficiency of approximately 9%. For the final analysis, a kinematic fit will be used to improve momentum resolution and help remove background from the invariant mass signals.

4.2.2 Beam time request

It is desired to measure the beam asymmetry, Σ, to a precision of at least 0.05 (absolute value). This is consistent with the precision of the previous measurements of Ewald *et al.* [16] and allows the determination of the sign of Σ to values smaller than 0.1. It was calculated that 1000 events per energy and theta bin were required to meet this criteria.

An analytic calculation of the degree of polarisation [28] was used to calculate the number of polarised photons for a given polarised peak position over the range where the polarisation exceeded 30%. Over the range of interest between 1680 - 1845 MeV, the photon flux of polarised photons is given as $N_\gamma = 2.53 \times 10^5 \text{s}^{-1}$.

Using the same notation as in section 4.1.2:

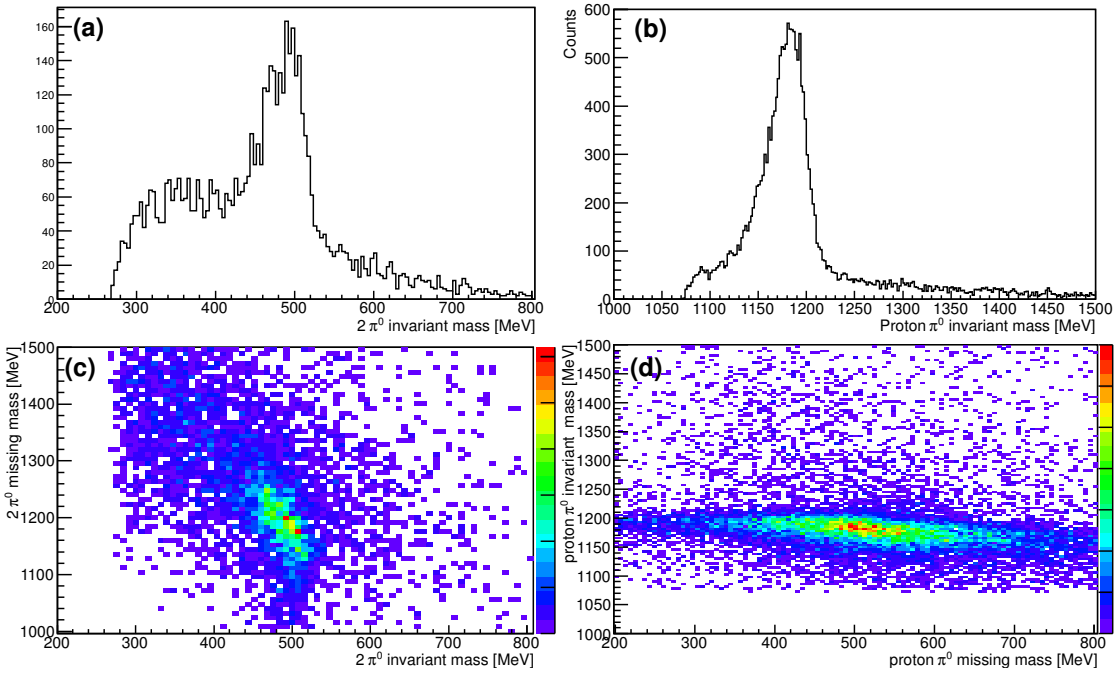

Figure 13 (a) K^0 invariant mass reconstructed from $K^0 \to \pi^0\pi^0$ (b) Σ^+ invariant mass reconstructed from $\Sigma^+ \to p\pi^0$. (c) $2\pi^0$ invariant mass (K^0) versus the missing mass mass Σ^+. (d) $p\pi^0$ invariant mass (Σ^+) versus the missing mass (K^0).

- $N_\gamma = 2.53 \times 10^5 \mathrm{s}^{-1}$;
- N_θ = 5;
- N_W = 2;
- C = counts per bin required = 1000;
- $d\sigma/d\Omega$ = 0.04μb;
- ρ_T = 0.2558 b^{-1};
- $\epsilon_{eff} = 0.09 \times 11.9$ (detection efficiency multiplied by the solid angle of acceptance)

The estimated beam time required, t is given as:

$$t = \frac{CN_\theta N_W}{(d\sigma/d\Omega)N_\gamma \rho_T \epsilon_{eff} \epsilon_{DAQ}}$$

A beam time of 2000 hours (83 days) using a crystal radiator to produce polarised beam with a maximum polarisation peak at 1.8 GeV is therefore requested.

5 Beam request summary

- 1000 hours of an unpolarised electron beam at an energy of 3.2 GeV. A copper radiator will be used to produce energy tagged unpolarised photons up to an energy of 2.88 GeV.
- 2000 hours of an unpolarised electron beam at an energy of 3.2 GeV. A crystal radiator will be used to produce linearly polarised beam with a maximum polarisation peak at 1.8 GeV.

6 Outlook

The beam time requested in this proposal is for the first part of an extensive associated strangeness photoproduction series of measurements. The photoproduction of K^0 from neutrons (deuteron target) and investigations of poorly understood or missing hyperon states will comprise the second part of the programme. These analyses will rely on analysis techniques refined in the first part of the programme. The physics motivations are described below.

6.1 $\gamma n \to K^0\Lambda$

Determining s-channel resonances contributing to the $\gamma p \to K^+\Lambda$ spectrum is complicated by large t-channel contributions. K^0 photoproduction in this sense is easier to understand due to the absence of t-channel K^0 exchange. Furthermore, $\gamma n \to K^0\Lambda$ provides a crucial constraint in understanding the reaction mechanism for $\gamma p \to K^+\Lambda$ as the hadronic coupling constants are linked via SU(3) symmetry. Measurements and the extraction of polarisation observables for this channel is therefore mandatory to determine the photoproduction mechanism. Despite this there is insubstantial data available.

The first cross section data for $\gamma n \to K^0\Lambda$ using a deuterium target was measured with the Neutral Kaon Spectrometer at the Laboratory of Nuclear Science (LNS) at Tohoku University [29]. The experiment had an acceptance of approximately π steradians, covering forward angles up to a photon beam energy of 1.1 GeV. K^0 were identified via the decay $K^0 \to \pi^+\pi^-$, where the K^0 invariant mass was reconstructed from pion momenta. Fig 14 shows the measured cross section for the inclusive reactions $\gamma N \to K^0 Y$ (where Y is either Λ, Σ^0 or Σ^+). The data suggests a more backward peaking angular distribution than what was predicted with the Kaon-MAID parameterisation [17].

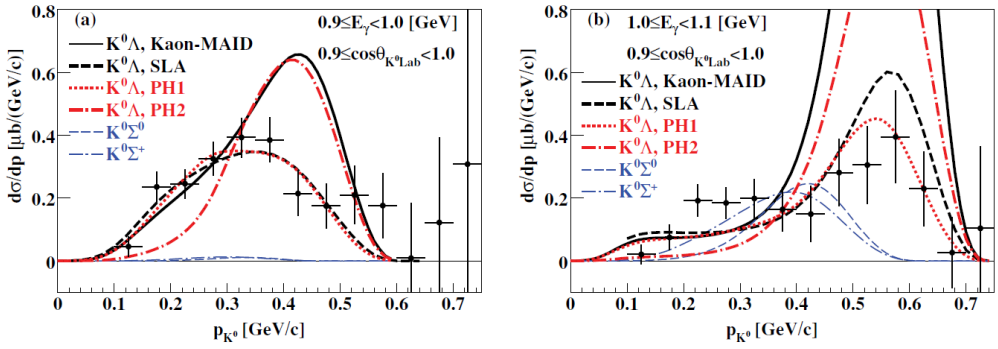

Figure 14 $\gamma(n, K^0)\Lambda$ differential cross section as a function of K^0 momentum for photon beam energy (a) 0.9-1.0 GeV and (b) 1.0-1.1 GeV, for laboratory frame polar angles smaller than 25^0. Solid black line is a Kaon-MAID fit [17], dotted black line the Saclay-Lyon A isobar model [30], dotted red and dot-dashed red are phenomenological models described in [29], and the blue dashed and dot dashed lines are Kaon-MAID fits to $K^0\Sigma^0$ and $K^0\Sigma^+$. Taken from [29].

The BGO-OD will be able to measure detailed differential cross section data for this channel, from threshold to 2.8 GeV photon beam energy and over nearly 4π steradians. The identification of multiple decay channels will vastly improve existing statistics. Using circularly and linearly polarised polarised photon beams, the polarisation observables, Σ, O_X, O_Z, C_X, and C_Z will also be extracted.

6.2 Hyperon photoproduction

This section highlights future proposals with the BGO-OD for the investigation of hyperon excited states (Y^*). The charged and neutral kaon identification which has already been discussed is intended to be the foundation of this research. The BGO-OD capability of the identification of mixed charge final states, and acceptance at very forward angles allows the determination of Y^* via multiple channels and decay modes.

6.2.1 $\Lambda(1405)$

Recent advances in chiral unitary formalism for meson baryon interactions [31, 32, 33] described the $\Lambda(1405)$ as a two-pole structure, with the contributions interfering on the real energy axis. The $\Lambda(1405)$ can only be observed via the decays: $\Lambda(1405) \rightarrow \pi\Sigma$ with $I = 0$, however it was found that there is different coupling of the two poles to different meson-baryon channels, leading to a difference in the $\Lambda(1405)$ line shape depending upon the decay it is observed via.

The $\Lambda(1405)$ mass was reconstructed from all three decay modes using recent data from the CLAS detector [34]. It is clear that the line shape differs depending upon the decay mode, however they do not agree with theoretical predictions where the $\Sigma^-\pi^+$ line shape is at a higher mass.

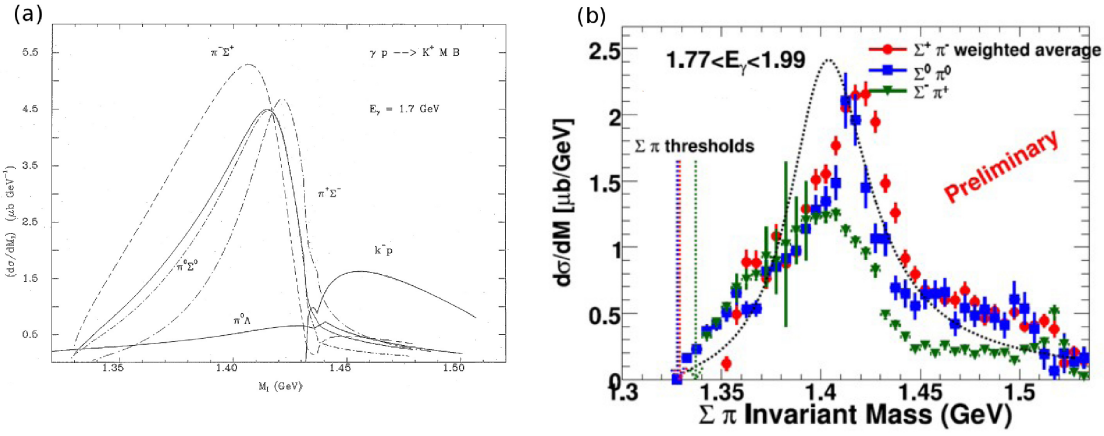

Figure 15 (a) The predicted $\Lambda(1405)$ lineshape for different decay channels (inset) as predicted by a chiral unitary formulism [31, 32, 33]. Taken from [33]. (b) The measured $\Lambda(1405)$ line shape for all decay channels (inset) with the CLAS detector [34]. The dashed line is a relativistic Breit-Wigner shape using mass and width values from the PDG. Taken from [34].

6.2.2 Missing and poorly understood hyperon states

Constituent quark models with three quenched quark states cannot accurately describe the mass differences of excited hyperons. The lowest excitation energy of a baryon of approximately 450 MeV is too high to describe the $\Lambda(1405)$, and the mass difference to the spin orbit partner, $\Lambda(1520)$ is too large. It is also difficult to reconcile the $\Lambda(1405)$ mass to be lower than the non-strange $N(1535)$.

These mass differences however can be described using unquenched quark models with five components [35, 37, 38]. These can either be interpreted as a meson cloud or a pentaquark molecule with di-quark structure. The $N^*(1535)$ for example can be described as a bound $K\Lambda - K\Sigma$ system and $\Lambda(1405)$ as a dynamically generated $KN - \Sigma\pi$ resonance. Alternatively within a penta-quark description, $N^*(1535)$ can be described as $[ud][ud]\bar{d}$ and $\Lambda(1405)$ as $[ud][sq]\bar{q}$ with $q\bar{q} = (u\bar{u} + d\bar{d})/\sqrt{2}$. These descriptions have important implications for the entire spectrum of hyperon resonances. Within the penta-quark model for example, a Σ^* with $J^\pi = 1/2^-$ is expected close in mass to $\Sigma(1385)$. The current knowledge of excited hyperon states is relatively poor, with the majority of data measured before 1980 with limited statistics. There are, for example, no PDG assigned four star $J^\pi = 1/2^-$ states for Σ^*, Ω^* hyperons.

Old data (pre 1980) for $K^-p \rightarrow \Lambda\pi^+\pi^-$ [36] has been re-examined in a search for Σ^* states with $J^\pi = 1/2^-$ [38], in light of a potential $\Sigma^*(1/2^-)$ structure observed in J/ψ decays [37]. A fit to the $\Lambda\pi^-$ mass spectrum favours the inclusion of a second resonance close in mass but with a width of approximately 120 MeV. Including the second resonance also improves the fit to the angular distribution between the incident K^- and Λ (the $\Sigma(1385)$ with $J = 3/2^+$ gives an angular distribution of the form $(1 + 3\cos^2\theta)/2$, and the addition of a resonance with $J = 1/2$ gives a flat distribution component).

Wu, Dulat and Zou [35] proposed that the existence of a $\Sigma^*(1/2^-)$ state close to the $\Sigma(1385)$ can be tested via the decay $\Lambda(1520) \rightarrow \Sigma^*\pi \rightarrow \Lambda\pi^+\pi^-$. The $\Lambda\pi^-$ invariant mass is sensitive to the inclusion

of the extra resonance due to the final state particles being either in relative P-wave or S-wave for $\Lambda(1520) \rightarrow \Sigma^{*+}_{3/2}\pi^-$ and $\Lambda(1520) \rightarrow \Sigma^{*-}_{1/2}\pi^+$ respectively. Model fits to data were promising, however it concluded that higher statistics data is required to establish this resonance.

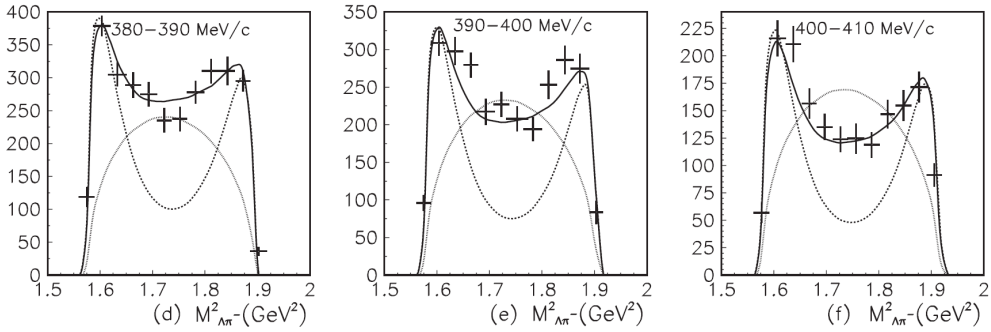

Figure 16 $\Lambda\pi^-$ invariant mass for different K^- momenta (inset) for the reaction $K^-p \rightarrow \Lambda\pi^-\pi^+$. Data from [?], lines are model fits from Wu *et al.* [35] when only including $\Sigma(1385)$ (dotted line) and also including a $\Sigma^*_{1/2}$ (solid line) and a phase space distribution (thin line). Figure adapted from [35].

The LEPS collaboration measured differential cross section and beam asymmetry data for $K^+\Sigma^{*-}$ photoproduction off the deuteron [39]. The beam asymmetries were small and negative, in contrast to the positive values predicted by Oh, *et al.* [40], who included weakly established resonances predicted by quark models to accurately describe cross section data.

Recent analysis of previous Crystal Ball data for $K^-p \rightarrow \pi^0\Lambda$ [41, 42] fitted effective Lagrangians to differential cross sections and Λ polarisation data. After including t-channel K^* exchange, u-channel proton exchange and four star Σ resonances, the best fit to data required an extra Σ resonance with $J^\pi = 1/2^+$, mass 1635 MeV and width 120 MeV.

Due to the limited data on excited hyperons and the ambiguity as to their structure, a detailed search with the BGO-OD experiment is proposed. Σ^* resonances close in mass to $\Lambda(1405)$ can be identified via $\Sigma^* \rightarrow \pi\Lambda$, and avoid misidentified background from $\Lambda(1405)$. Differential cross sections, and polarisation observables, Σ, P, C_X and C_Z will be used to disentangle reaction mechanisms. Resonant structure can be studied via the photoproduction of K^*, K^+ and K^0. The reaction $\gamma p \rightarrow K^+\Lambda(1520)$ will also be studied to constrain potential $\Sigma^*_{1/2}$ resonances close to $\Sigma(1385)$, and provide differential cross section data up to 2.8 GeV. The BGO-OD experiment will identify all three $\Lambda(1405)$ decay modes, providing differential cross section, and t dependence data for each. The experimental setup is ideal to identify all particles in the final state for the decay $\Lambda(1405) \rightarrow \Sigma^0\pi^0$, the only decay channel with no background from $\Sigma(1385)$ (isospin forbidden).

7 References

[1] S. Capstick and W. Roberts, Phys. Rev. D **58**, 074011 (1998)

[2] K. H. Glander *et al.*, Eur. Phys. J. A **19**, 251 (2004)

[3] M. Q. Tran *et al.*, Phys. Rev. Lett. B **445**, 20 (1998)

[4] R. Bradford and R. A. Schumacher *et al.* (CLAS Collaboration), Phys. Rev. C **73**, 035202 (2006)

[5] J. C. W. McNabb *et al.* (CLAS Collaboration), Phys. Rev. C **69** (2004) 042201

[6] T. Mart, Int. J. Mod. Phys. E **19**, 2343 (2010)

[7] M. Sumihama *et al.* (LEPS Collaboration), Phys. Rev. C **73** (2006) 035212

[8] M. E. McCracken, M Bellis, C. A. Meyer, M Williams *et al.*, Phys. Rev. C **81** (2010) 025201

[9] V. Kuznetsov *et al.*, Phys. Lett. B **647**, 23 (2007)

[10] I. Jaegle *et al.* (The CBELSA/TAPS Collaboration), Phys. Rev. Lett **100**, 252002 (2008)

[11] M.V. Polyakov and A. Rathke, Eur. Phys. J. A **18**, 691 (2003)

[12] V. Shklyar, H. Lenske and U. Mosel, Phys. Lett. B **650**, 172 (2007)

[13] T. Mart, Phys. Rev. D **83**, 094015 (2011)

[14] V. D. Burkert, Meson 2012 proc. arXiv:1209.2402v1 [nucl-ex] (2012)

[15] B. Dey, PhD Thesis, Carnegie Mellon University (2011)

[16] R. Ewald *et al.*, Phys. Lett. B **713** (2012) 180

[17] T. Mart, C Bennhold, H Haberzettl and L Tiator, wwwkph.kph.uni-mainz.de/MAID//kaon/ (2010)

[18] R.A. Arndt et al., http://gwdac.phys.gwu.edu

[19] M. Nanova et al. (Crystal-Barrel/TAPS Collab.), Eur. Phys. J. A **35** (2008) 333

[20] E. Oset and A. Ramos, Eur. Phys. J. A **44** (2010) 445

[21] R. Castelijns *et al.*, Eur. Phys. J. A **35** (2008) 39

[22] R. Lawall *et al.*, Eur. Phys. J. A **24** (2005) 275

[23] O.Bartalini et al., Eur.Phys.J. A26 (2005) 399-419

[24] P. Levi Sandri et al., Nucl. Instrum. Methods Phys. Res. A 370 (1996) 396-402

[25] F. Ghio et al., Nucl. Instrum. Methods Phys. Res. A 404, (1998) 71-86

[26] M. Castoldi et al., Nucl. Instrum. Methods Phys. Res. A 403,(1998) 22-30

[27] http://geant4.cern.ch

[28] A. Bella, Diploma Thesis, University of Bonn (2012)

[29] K. Tsukada *et al.*, Phys. Rev. C **78** (2008) 014001

[30] T. Mizutani, C. Fayard, G. H. Lamot and B. Saghai Phys. Rev. C **58** (1998) 75

[31] T. Hyodo and D. Jido, Prog. Part. Nuc. Phys. **67** (2012) 55

[32] D. Jido, J. A. Oller, E. Oset, A. Ramos and U. G. Meissner, Nuc. Phys. A **725** (2003) 181

[33] J. C. Nacher, E. Oset, H. Toki, A. Ramos and U. G. Meissner, Phys. Lett. B **455** (1999) 55

[34] K. Moriya and R. Schumacher (CLAS Collaboration), Nuc. Phys. A **835** (2010) 325

[35] Jia-Jun Wu, S. Dulat and B. S. Zou, Phys. Rev. C **81** (2010) 045210

[36] D. O. Huwe, Phys. Rev. **181** (1969) 1824

[37] B. S. Zou, Int. J. Mod. Phys. **21** (2006) 5552

[38] Jia-Jun Wu, S. Dulat and B. S. Zou, Phys. Rev. DD **80** (2009) 017503

[39] K. Hicks, D. Keller, H. Kohri *et al.* (LEPS Collaboration), Phys. Rev. Lett. **102** (2009) 012501

[40] Y. Oh, C. M. Ko and K. Nakayama, Phys. Rev. C **77** (2008) 045204

[41] S. Prakhov *et al.* (Crystal Ball Collaboration), Phys. Rev. C **80** (2009) 025204

[42] P. Gao, B. S. Zou, A. Sibirtsev, Nuc. Phys. A **867** (2011) 41